A new way to study geomagnetic storms

James Hutchinson and colleagues describe a novel radar technique to study geomagnetic storms: superposed latitude–time–velocity plots. This is a summary of the poster winning one of the Rishbeth Prizes at the NAM/UKSP/MIST meeting in April.

Space is not empty. The solar wind (SW) carries millions of tonnes of energetic particles outward from the Sun each second which, along with the embedded interplanetary magnetic field (IMF), exerts a strong influence on our own geospace. Usually we are protected by our own magnetic shield called the magnetosphere. However, geomagnetic storms – defined by periods of intense solar wind–magnetosphere coupling in association with extreme SW conditions, usually coronal mass ejections (CMEs) or co-rotating interaction regions (CIRs), which cause large global disturbances in the Earth's magnetosphere (Gonzalez *et al.* 1994) – deposit huge amounts of energy into the magnetosphere. One manifestation of this is the aurora (or northern lights), a ring or oval of emission centred on the magnetic poles when viewed from space, caused by the interaction of the neutral atmosphere and energetic particles trapped in the Earth's magnetic field. Recent headlines such as "Space storms threaten technology" (http://www.bbc.co.uk/news/world-us-canada-12516918, accessed 15/06/2011) and "Solar storms could create $2 trillion 'global Katrina' " (http://www.guardian.co.uk/science/2011/feb/21/solar-storms-global-katrina, accessed 15/06/2011) highlight the importance of understanding this interaction. With society's ever growing dependence on satellite applications such as the Global Positioning System, satellite communications and TV, along with the threat of damage to our national power grids through geomagnetic induced currents (GICs, Turnbull 2010), the need to understand and predict the effects of space weather are of vital importance.

The magnetosphere, magnetic reconnection and the Dungey cycle

The magnetosphere is a region in spaced formed by the draping of the SW and IMF on our own terrestrial dipole magnetic field and ionospheric plasma (see figure 1 in "Blowing in the solar wind" on page 4.XX of this issue). Initially the magnetosphere was considered a closed system, meaning solar wind plasma could not enter the near-Earth region. However, the two do interact: the solar wind crashes into the dayside terrestrial field causing it to be compressed and then flows around the Earth's field, dragging it into an elongated tail-like structure called the magnetotail. Under certain conditions, usually associated with a southward orientation of the IMF (usually quoted in three components: X in the Sun–Earth line, Z is in the direction of the northern magnetic pole and Y perpendicular to both), a process called magnetic reconnection can occur, opening the Earth's dipole field to the IMF and allowing the transport of energetic solar particles into the system. These open field lines and plasma convect across the magnetic poles with the flow of the solar wind and are stored in the magnetotail until a second point of magnetic reconnection occurs, reclosing the terrestrial field and the field lines convect back to the dayside at low latitudes.

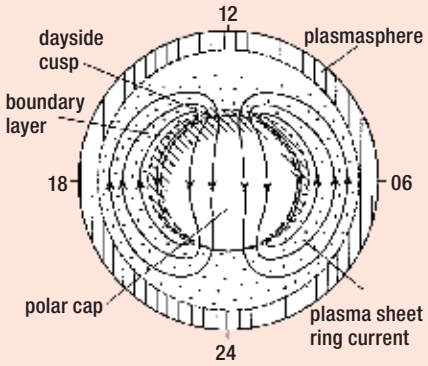

1: View looking down on the northern high-latitude ionosphere, labelling the footprints of key aspects of the magnetosphere and showing the plasma flows in solid arrows in the classic twin cell convection pattern of the Dungey cycle. (Adapted from Cowley 1993)

This repeatable cycle is known as the Dungey cycle (1961) and repeats with the natural variation in the IMF from positive to negative values of B_Z, resulting in the footprints of the magnetic field lines tracing a well known twin-cell convection pattern (figure 1) that can easily be observed by the Super Dual Auroral Radar Network (SuperDARN) via backscatter off the flows of plasma on these field lines. Auroral images are also often used as a proxy for the size of the open region of the magnetosphere via the dim region within the main aurora and can be used to find the open–closed boundary (OCB). The expansion, a sudden broad brightening in the pre-midnight sector and subsequent recovery of the auroral oval, is also a clear indication of the substorm cycle: the fundamental global disturbance of the Dungey cycle where stored energy in the magnetotail from prolonged magnetic reconnection on the dayside is suddenly and explosively released every few hours causing vivid auroral displays. However, times of extreme solar wind–magnetosphere coupling can cause reconnection at a rate far greater than can be recovered by the substorm cycle, forming a geomagnetic storm that among other effects causes enhanced auroral displays, radiation belts and ring current, with the latter particularly useful in the identification of these storms. We use a combination of datasets to present a new superposed epoch analysis technique for SuperDARN radar data during geomagnetic storms.

Identifying geomagnetic storms

Geomagnetic storms are identified via a characteristic SYM-H index trace (figure 2), a high-cadence index to observe geomagnetic activity created using a network of magnetometers positioned around the Earth's equator to measure tiny deflections in the terrestrial magnetic field strength caused by the induced field from the ring current – the flow of ions and electrons associated with the aurora. The SYM-H index trace consists of three distinct phases: initial, main and recovery phase. The initial phase is a small positive increase in SYM-H associated with the squeezing of the dayside terrestrial magnetic field by increased SW ram pressure from the solar eruption or fast stream. With the onset of favourable IMF conditions, namely a southward IMF orientation, enhanced dayside magnetic reconnection can occur, enlarging the polar cap, and in turn convecting large amounts of energy into the magnetotail, exciting the radiation belt and ring-current plasma. This increase in ring-current particle energy and

density induces a magnetic field that opposes the terrestrial one, causing a sharp negative drop in the SYM-H index and identifies the main phase. The recovery phase is shown in the gradual return of SYM-H to normal values via ring-particle losses (usually taking days) and scattering out of the system; the onset of recovery is usually associated with a reduction in the enhanced SW driving conditions or a positive or northward tuning of the IMF B_Z component.

Unanswered questions...

There are still several unanswered questions concerning geomagnetic storms, particularly in the relationship between duration and size of storms, important in understanding space weather effects as well as the mechanisms of excitation and decay of the ring current. Here we are addressing the first question, using a combination of radar data and auroral images as a proxy for the amount of coupling and energy input to the magnetosphere during different intensity storms. This is in addition to a previously completed statistical study of 143 geomagnetic storms over the most recent solar cycle (1997–2008) and their associated SW conditions through parameters such as SW speed, pressure, density and IMF components which showed that both the relative size and duration of SW enhancement was important in determining how large a storm can become. This means that the most intense storms can occur on the same timescales as the weakest, making the prediction of hazardous events difficult. We superpose events to the average duration of each phase (initial, main and recovery) for each storm size category rather than a simple t_0 start time alignment, essentially stretching and compressing the timestamp of the data to give a better alignment of "like" features in the naturally variable storm progression (seen in figure 3).

SuperDARN and IMAGE

SuperDARN (Greenwald *et al.* 1995) is an international array of high-frequency coherent-scatter radars, currently consisting of 19 northern and 9 southern hemisphere radars with their fields-of-views (FOV) covering a significant proportion of both auroral and polar regions of the ionosphere (each FOV has an estimated area of ~4 million km^2). Doppler-shifted backscatter is received from ionospheric plasma irregularities when the Bragg scattering condition is met, with autocorrelation functions constructed to extract parameters such as signal-to-noise power, velocity and spectral width. Ground-scatter can be identified and removed based on characteristic magnitudes of velocity and spectral width (Ruohoniemi and Baker 1998). While backscatter from individual radars can be investigated, the true power of SuperDARN is in the use of multiple radars with overlapping FOV, allowing the estimation of the distribution of the electrostatic

2: The characteristic SYM-H index trace of a geomagnetic storm showing the initial, main and recovery phases

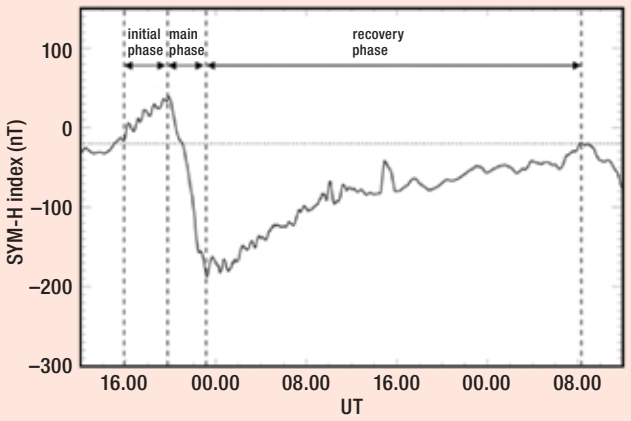

3: Diagram of the superposition method using a normalized timeline.

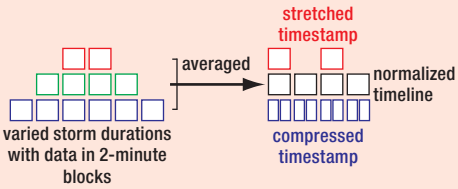

4: Example of superposed 2-minute period of radar backscatter using the map potential technique on geomagnetic storm periods discussed.

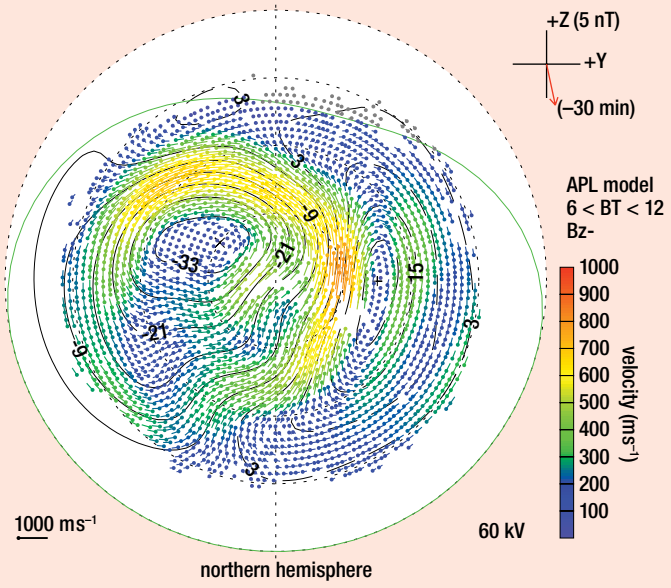

5: Example of superposed auroral images to match the 2-minute period of figure 4 from the IMAGE spacecraft.

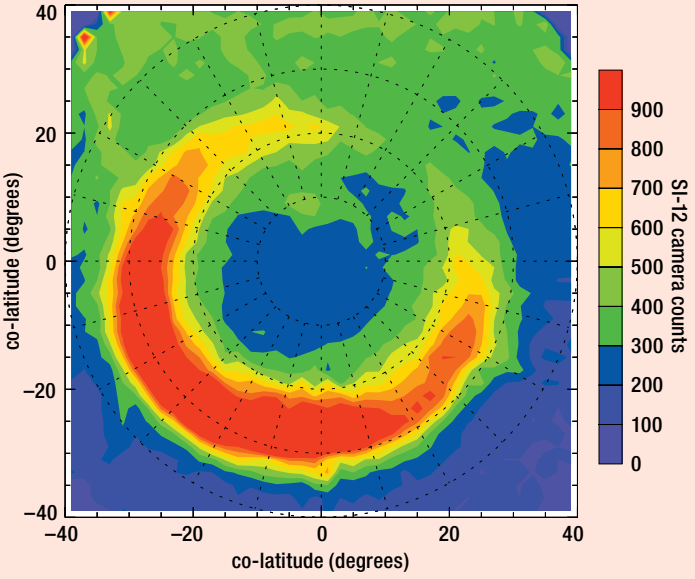

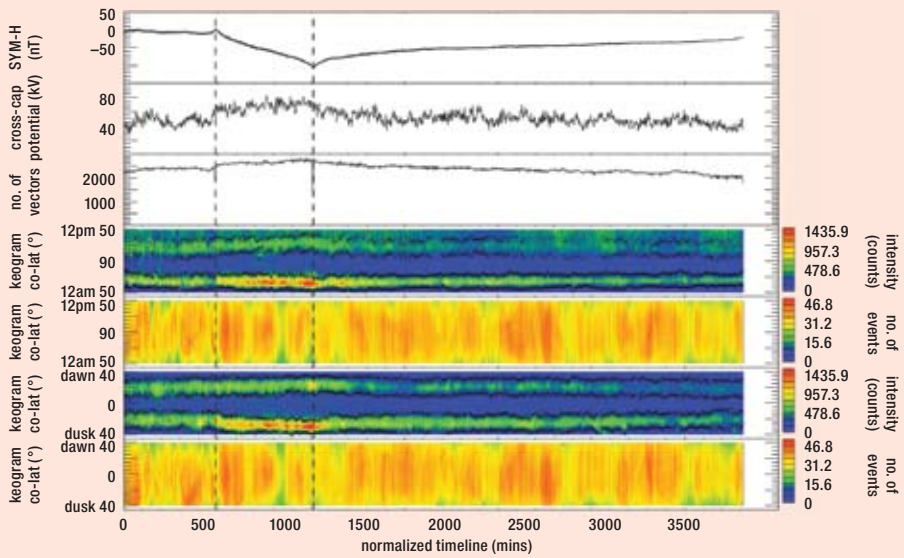

6: Small storm superposed epoch results showing SYM-H, cross-cap potential, the number of vectors involved in the map potential modelling, day–night and dawn–dusk auroral keograms and the number of images involved in each 2-minute/2° magnetic latitude.

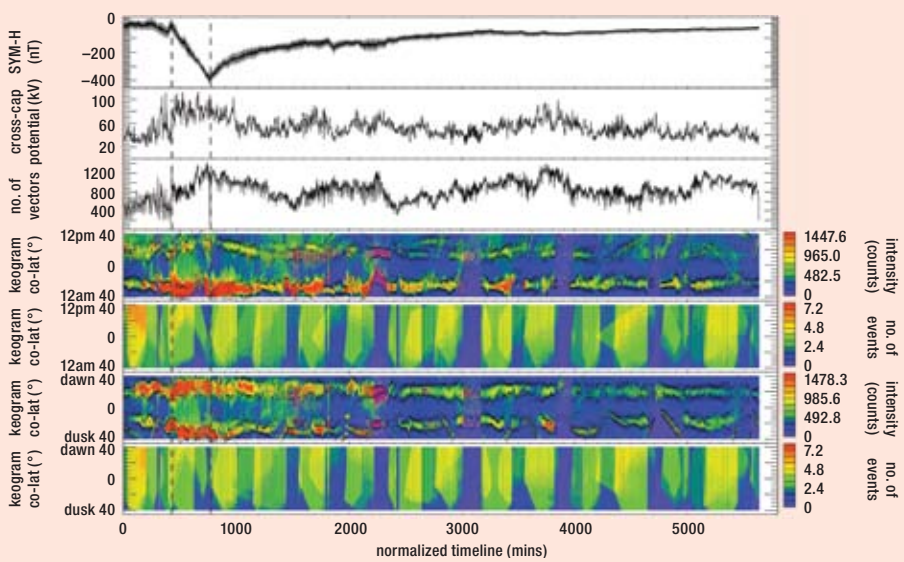

7: Large storm superposed epoch results showing SYM-H, cross-cap potential, the number of vectors involved in the map potential modelling, day–night and dawn–dusk auroral keograms and the number of images involved in each 2-minute/2° magnetic latitude.

potential or global convection electric field, which controls the flow of ionospheric plasma (often called the cross-polar cap potential).

In addition to this, Ruohoniemi and Baker (1998) presented a method of combining multiple radars using the "map potential" technique. Here a global grid system of equi-area bins is created (1° magnetic latitude which is approximately 111 km mapped to the ground and 111 km in the longitudinal dimension) and the radars are mapped to this. An *n*th-order spherical harmonic model is then applied to the data allowing for estimates of the convection in regions where radar backscatter is absent. This technique of mapping to a fixed magnetic local time (MLT) clock system makes it possible to superpose events, removing the spatial/temporal issues of superposing data from individual radars. This technique has been put to good use in investigating the dynamics of substorms, which are known to closely control the convection seen, for example in Grocott *et al.* (2009) and references therein. However, the more general average dependence on geomagnetic storms has not been investigated in this way, perhaps making the current study the first statistical analysis of the average convection during geomagnetic storms.

Auroral images of storm time periods during the five-year mission of the Imager for Magnetopause-to-Aurora Global Exploration (IMAGE) spacecraft's Spectrographic Imager SI-12 camera (Mende *et al.* 2000) have been superposed to provide a complimentary dataset for analysis. Boakes *et al.* (2008) have shown that the auroral oval boundary can be identified in IMAGE SI-12 using a Gaussian fitting technique similar to that used by Carbary *et al.* (2003) for the POLAR spacecraft mission, allowing the identification of the open–closed boundary discussed earlier. Milan *et al.* (2009) showed a correlation between storm size (or ring current enhancement) in SYM-H and the radius of the auroral oval, again highlighting that while the substorm activity gives the general dependence on the auroral oval and polar convection, geomagnetic storms also have an additional influence.

Small vs large

Figures 6 and 7 show the results of the superposition of SYM-H, the calculated cross cap potential from the map potential technique (and number of radar vectors involved in the fit for each 2-minute period) and day–night and dawn–dusk keograms of the superposed IMAGE aurora (with number of events shown for each ~2-minute and 2° magnetic co-latitude bin). It has been shown that larger storms are associated with more extreme conditions in the SW, that in turn lead to increased SW coupling (Hutchinson *et al.* 2011) and an increase in the radius of the auroral oval and therefore polar cap area (Milan *et al.* 2009). This result is reproduced in figures 6 and 7 where we see an increase in the cross cap potential during the main phase of the storm seen in SYM-H, along with both a brightening and expansion of the aurora during this period. As might be expected, this is a larger increase in both cases for the more intense storm, though it should be noted that there are far fewer intense events which in turn leads to less smoothing of results from the averaging process. Despite this we see sufficient vectors (between ~1000 and 3000 for each 2-minute period) in the map potential technique to get a good fit, as well as sufficient averaging of auroral images that one event does not dominate.

It is interesting to note that for the intense storm results, subsequent expansions and brightening of the auroral oval are seen to coincide with smaller storms that occurred after the large main events. It should also be noted that the colour scale of the intensity of the auroral keograms has been set to saturate such that smaller intensities could be seen. In both figures the OCB has been found using the Gaussian fitting method described above, with a generally close fit shown to the poleward and equatorward boundaries of the auroral oval seen in black on figures 6 and 7. The Gaussians used in fitting were obviously much broader than is the case for an individual image file due to the nature of the averaging, requiring a slight adjustment in the requirements of FWHM[what's that?] of the fit from Boakes *et al.* (2008), with regions with no fit suggesting a poor superposition of images either due to small numbers of events or very dynamically different events. The fact

that the study has reproduced expected results (increased polar cap potential and a brightening and widening aurora during storm main phase) shows that the superposition technique is aligning "like" features in storm progression well, and that on average the substorm control on the convection and aurora is generally being averaged out, seen by the good fit of the average boundaries of the auroral oval, leaving the average effect of the storms.

Latitude–time–velocity plots

The latitude–time–velocity (LTV) plots technique uses the superposed map-potential data previously discussed and takes a keogram slice down a specific magnetic local time (MLT) to produce a plot of latitude against time with colour showing velocity. Two plots are produced to show the north–south and east–west components of the model vectors produced from the map-potential technique. In all cases north points to the northern magnetic pole and the easterly direction is perpendicular to this. They are analogous to a standard range–time–intensity plot that is common in visualizing SuperDARN radar data, but employ the map-potential technique of Ruohoniemi and Baker (1998) to both combine multiple radar data and allow superposition of events without complications due to the spatial/temporal issues with moving radar FOV. A 6th-order spherical harmonic model is fitted to the combined storm data after superposition, rather than to each individual event. The gridding technique compensates for any different operation modes used by the different radars.

Figure 8 shows an example of the 00:00 MLT LTV plot for small storms with a panel for the corresponding superposed SYM-H index showing the progress of the storm. Data is smoothed by a 10-minute averaging and the IMAGE OCB is shown in black on the keograms. In the V_N panel, red colour shows the anti-sunward cross cap flow of the twin cell convection (figure 1) down to approximately the centre of the auroral oval boundaries. The V_E panel shows westerly velocities in red poleward of the auroral boundaries, perhaps suggesting an overall IMF B_Y influence which would slightly twist the anti-sunward flow from being directly across the polar cap. Further work will include separating storms into mainly positive or mainly negative IMF B_Y components during storm main phase to observe this influence on the convection pattern (see Cowley and Lockwood 1992 for more details). The turning of the convection to the low-latitude return flows is seen within the auroral oval boundaries. Interestingly there are a couple of occurrences of strongly eastward flows at the poleward boundary and strongly westward flows at the equatorward boundary (particularly at the beginning of the main phase of the storm at 10–12 hrs) that might indicate the formation of the Harang discontinuity that occurs during substorm onset.

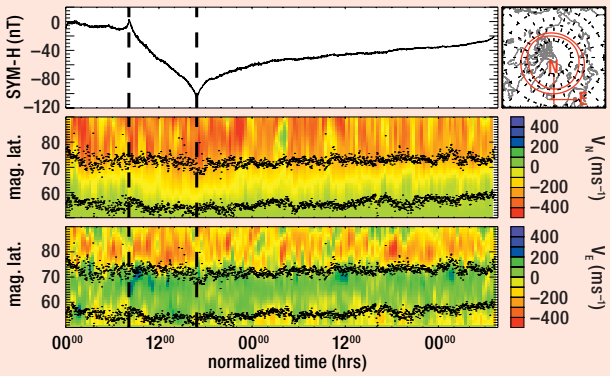

8: An example of the LTV plotting technique down the midnight meridian for north–south (VN) and east–west (VE) velocities, plotted with SYM-H and a diagram showing the look directions.

Though not shown here, there is some clustering of the Frey *et al.* (2004) substorm onset times after superposition to the geomagnetic storm normalized time index, which generally coincide with these strong easterly flows. Work is needed to investigate this further, but it would make sense for the first substorm after the onset of the main phase of a storm to align with other events as both require the IMF to turn to a southward direction. However, there is no reason for subsequent substorms to align particularly, and this results in an "averaging" of the substorm control on the global convection and lets us observe the superimposed geomagnetic storm control. In both panels we reproduce the results of figures 6 and 7 whereby the polar cap has expanded during storm main phase to lower latitudes, and again this is more pronounced on more intense storms.

Summary and future work

The application of the map potential technique to geomagnetic storms has shown some interesting results to date, including the expansion of the oval radius during the main phase of storms as shown by Milan *et al.* (2009) and an increased polar cap potential during this time as might be expected. Substorm effects have generally been smoothed, though there is some evidence of the Harang discontinuity at the onset of the main phase of storms. An unexpectedly good fit of the OCB location from the IMAGE aurora to the SuperDARN data is seen for small storms, showing that the superposition technique is working well to give the average effects of geomagnetic storms on convection. The fact that this fit worsens for more intense storms is likely due to the small numbers of significantly variable events that are averaged.

Future work will involve separating storms by IMF B_Y component to observe this influence on the convection, as well as looking further at the alignment of substorms during storm time conditions. Also of interest is the dusk–midnight sector of the convection, where substorm dominance of the control has led to a less smooth averaging of the flows, suggesting a dual return flow at low latitudes that is unlikely to be a real effect and rather two more likely return flow locations based on some other controlling mechanism. An index is required to show how much radar data constrains the model fitting technique at a given MLT and magnetic latitude, as well as a breakdown of how the different radars contribute with events and MLT – magnetic latitude. This could then lead on to statistical studies of the occurrence of radar echoes using map-potential techniques for superposition, which can be compared to previous studies such as Kane and Makarevich (2009) that have tried to use "quiet time" curves to subtract from storm time scatter to look at the statistical occurrence of radar echoes during storms. It is hoped that this new technique will complement our previous statistical study of geomagnetic storms over the last solar cycle (Hutchinson *et al.* 2011) and provide a new insight into the global convection and flow of energy during geomagnetic storms. ●

J A Hutchinson, D M Wright, S E Milan, A Grocott and P D Boakes, Dept of Physics and Astronomy, University of Leicester, UK; jh251@ion.le.ac.uk.

References

Boakes P D *et al.* 2008 *Ann. Geophys.* **26(9)** 2759–2769 doi:10.5194/angeo-26-2759-2008.
Carbary J F *et al.* 2003 *J. Geophys. Res.* **108(A1)** doi:10.1029/2002JA009378.
Cowley S W H and M Lockwood 1992 *Ann. Geophys.* **10** 103–115.
Dungey J W 1961 *Physical Review Letters* **6** 47–48.
Frey H U *et al.* 2004 *J. Geophys. Res.* **109(A10)** doi:10.1029/2004JA010607.
Gonzalez W D *et al.* 1994 *J. Geophys. Res.* **99(A4)** 5571–5792.
Greenwald R A *et al.* 1995 *Space Sci. Rev.* **71(1–4)** 761–796 doi:10.1007/BF00751350.
Grocott A *et al.* 2009 *Ann. Geophys.* **27(2)** 591–600 doi:10.5194/angeo-27-591-2009.
Hutchinson J A *et al.* 2011 Geomagnetic storms over the last solar cycle: a superposed epoch analysis *J. Geophys. Res.* (submitted).
Kane T A and R A Makarevich 2009 *J. Geophys. Res.* **115(A7)** doi:10.1029/2009JA014974.
Mende S E *et al.* 2000 *Space Sci. Rev.* **91** 287–318.
Milan S E *et al.* 2009 *Ann. Geophys.* **27(7)** 2913–2924 doi:10.5194/angeo-27-2913-2009.
Ruohoniemi J M and K B Baker 1998 *J. Geophy. Res.* **103(A9)** 20797–20811 doi:10.1029/98JA01288.
Turnbull K 2010 *A&G* **51** 5.25–5.26 doi:10.1111/j.1468-4004.2010.51525.x.